Proceedings of the 4th International Conference on Computing Innovation and Applied Physics
DOI: 10.54254/2753-8818/83/2025.19926

A High-Sensitivity Strain Sensor with Auxetic and Wrinkled Structure for Human Joint Motion Tracking

Dongning Lyu[1,a,*]

[1]*Guangzhou Huamei Bond International College, Guangzhou, China*
a. 1120130671@qq.com
**corresponding author*

Abstract: Capacitive strain sensors play a crucial role in tracking human joint motion. However, for a long time, the sensitivity GF of the strain sensor is theoretically limited to 1 and is difficult to improve under low strain. This study aims to enhance the sensitivity for more accurate joint motion monitoring by utilizing an auxetic structure (rotating squares system) combined with a wrinkled design to replace the traditional dielectric layer. This novel approach leverages the negative Poisson's ratio property of auxetic materials. In this study, inorganic silica gel (SiO_2) and conductive fabric are used to fabricate the dielectric layer and the electrodes, respectively. The strain sensor ($80.0mm * 20.0mm * 1.0mm$) with the proposed design achieves a maximum GF of 10.83 and a minimum GF of 4.07. Finally, the strain sensor is tested by measuring the bending angles of the knee joint during walking, jumping, a jump shot, and a fadeaway.

Keywords: capacitive strain sensor, flexible wearable device, auxetic structure, wrinkled structure, joint motion tracing.

1. Introduction

With the development of flexible electronics and sensing technology, flexible wearable devices have been widely applied in various field. In the field of sports, flexible wearable devices are primarily used for injury prevention and sports rehabilitation. These devices can monitor data such as an athlete's gait, speed, and strength to help adjust training plans and improve performance. Gait analysis, for example, can identify issues in an athlete's posture while running or walking and provide corrective suggestions to enhance movement efficiency.[1,2] Additionally, for injury prevention, wearable devices can monitor parameters like joint angles, velocity, and acceleration to identify potential injury risks. For example, abnormal movement patterns in the knee may signal an imminent injury. By providing early warnings, these devices allow athletes to adjust their movements in time to avoid injury.[3] In sports rehabilitation training, wearable devices can provide personalized training programs for patients, offering real-time feedback on their progress to ensure the rehabilitation process is both scientific and effective. For example, using wearable devices can help reduce the incidence of muscle atrophy.[4]

Among these, monitoring joint movements is crucial for both the prevention and rehabilitation of sports injuries. By tracking parameters such as joint angles, speed, and acceleration, it is possible to identify abnormal movement patterns and postures, allowing for timely corrections to prevent injuries. For example, a basketball player might suffer from muscle strains, joint damage, or even fractures

DOI: 10.54254/2753-8818/83/2025.19926

due to improper training techniques or overexertion during dribbling and rebounding. Furthermore, during rehabilitation, joint movement data can assist medical professionals in evaluating recovery progress and adjusting rehabilitation plans to ensure effective outcomes for patients.[5]

Flexible strain sensors, commonly classified into resistive-type and capacitive-type, are important for tracking joint motion. They are characterized by their light weight, simple read-out systems, cost-effectiveness, and high flexibility and stretchability.[6] Previous studies have indicated that compared to resistive strain sensors, while low-sensitivity and relatively complex to fabricate, capacitive strain sensors have the advantage of excellent linearity, hysteresis performance, and long-term repeatability, thereby being more suitable for long-time detection of human joint motion.[6,7]

The sensitivity (gauge factor) of capacitive strain sensors with normal configuration is theoretically limited to 1 due to the parallel-plate capacitor structure.[6,8] Therefore, sensitivity improvement of capacitive strain sensors has been a focal point, and several studies aim to increase the sensitivity through different materials and fabrication methods. Most of these methodologies were summarized by Amjadi et al. (2016).[6] However, for a long time, there have been few effective ways to improve the sensitivity of capacitive strain sensors when the strain applied to the sensor is relatively low, ranging from 0% to 20%. This limitation has become a major impediment in many application scenarios, particularly in tracking joint motion, where the strain generated by the human joint typically falls below this threshold. A study by Kim et al. (2017) has proposed that their strain sensor, with a gauge factor of 1.57 (absolute value), effectively detects strain from 0% to 30%, and it was the first research to optimize the gauge factor of capacitive-based strain sensors within this strain range. They patterned the Ag nanowire networks through the capillary force lithography method into electrodes with an interdigitated shape.[9] This result has greatly enhanced the accuracy of human joint motion measurements, but a gauge factor of 1.57 clearly implies room for further improvement. Nur et al. (2018) have designed a capacitive strain sensor with wrinkled ultrathin gold films that introduce an additional degree of freedom to the parallel plate capacitor. They achieved a GF of 3.05 at a maximum strain of 140%.[10] X. Hu et al. (2022) have demonstrated that utilizing wrinkled film structure and films of carbon nanotubes to replace metal films such as Au or Ag in sensors achieves a GF of 2.07 at 300% strain.[11] Both studies have proven the feasibility and reliability of using a wrinkled structure to overcome the theoretical maximum sensitivity. They have made crucial breakthroughs in increasing sensitivity under high strain, but neither has shown a notable change in GF under low strain.

Another approach successfully used in resistive strain sensors to reach high sensitivity, namely, auxetic materials, might provide valuable insights into enhancing capacitive sensor performance. Auxetics (metamaterials) are materials or structures with negative Poisson's ratio, which expand transversely under uniaxial tension. Integrating auxetic structures into strain sensors (both resistive-type and capacitive-type) can offset the negative influence of necking that occurs in sensors during the stretching process. Given that the negative Poisson's ratio property diminishes as the applied strain increases, auxetics are particularly suitable for enhancing sensitivity under mild strain.[12] Several studies have already exhibited the outstanding effectiveness of resistive-based strain sensors with auxetics. Lee et al. (2016) have developed a stretchable piezoresistive sensor using an auxetic foam with a Poisson's ratio of -0.5, which tremendously increased the gauge factor by 500%.[13] Taherkhani et al. (2020) have fabricated a low-strain sensitive piezoresistive sensor by blending silicone rubber with carbon fibers in an auxetic re-entrant structure, resulting in a gauge factor that reached up to approximately 28.[14] Wang et al. (2021) have also obtained an impressive result. They presented a high-performance auxetic bilayer conductive mesh piezoresistive strain sensor, which combines a SWCNT-coated stretchable silicone rubber mesh with a high-hardness auxetic frame, achieving a gauge factor of approximately 13.4—6.6 times greater than that of conventional sensors.[15] These studies strongly illustrate the remarkable function of auxetics in improving the

DOI: 10.54254/2753-8818/83/2025.19926

sensitivity of resistive-based strain sensors and highlight the possibilities for similar advancements in capacitive strain sensor research.

The objective of this study is to enhance the sensitivity of capacitive sensors at lower strain levels for tracing human joint motion. Two key elements are incorporated: an auxetic structure (rotating square system) with a negative Poisson's ratio and a wrinkled structure. The auxetic structure increases the surface area of the electrodes (one of the important factors directly influencing the sensitivity), while the wrinkled structure compensates for the reduced stretchability caused by auxetic design (well explained in Experiment). This novel strategy combines and maximizes the advantages of the auxetic and wrinkled structure, thereby effectively improving the sensitivity. Connected via Bluetooth, it enables real-time or offline data collection. A series of experiments are conducted, where the sensor is used for measuring the knee-bending angles during walking, jumping, a jump shot, and a fadeaway.

2. Methodology

2.1. Mechanism

2.1.1. Basic Structure of the Proposed Capacitive Strain Sensor

The suggested capacitive strain sensor adopts a sandwich-like structure, as seen in Figure 1. The dielectric layer is designed with an auxetic structure, and an ultrathin film, slightly longer than the dielectric layer, is applied to the bottom of the dielectric layer to form a wrinkled structure. Consistent with the conventional design, the dielectric layer is positioned between the positive and negative electrodes.

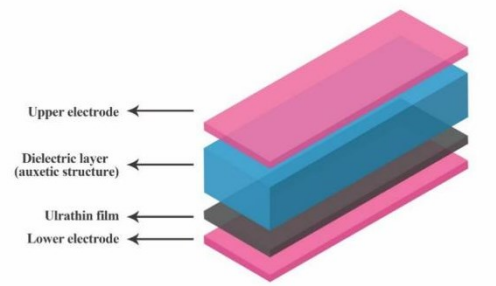

Figure 1: Proposed structure of the strain sensor

2.1.2. Auxetic Structure

The design of the auxetic structure is based on the rotating squares model, which was well-studied by Mizzi et al. (2015).[16] The deformation mechanism of this model is displayed in Figure 2.

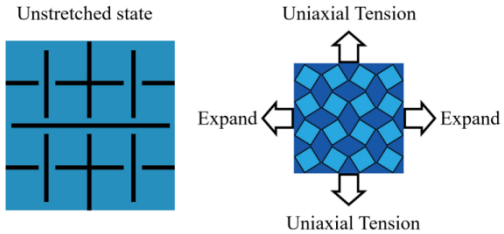

Figure 2: Rotating squares system

DOI: 10.54254/2753-8818/83/2025.19926

When uniaxial tension is applied, each square rotates transversely, thereby expanding the entire auxetic structure. As the auxetic structure expands, the width of the strain sensor (electrode) increases, resulting in a larger surface area, and the thickness decreases drastically (explained more clearly in Capacitive Model) because the sensor is primarily composed of inorganic silica gel, which can be assumed to be an isotropic, incompressible hyperelastic material. For traditional strain sensor, the width decreases when stretched, so the changes in surface area and thickness are not obvious. Therefore, the use of the auxetic structure allows the change in capacitance ΔC being measured to increase. (Capacitive Model explicitly discuss the relationship between the capacitance and the surface area and thickness).

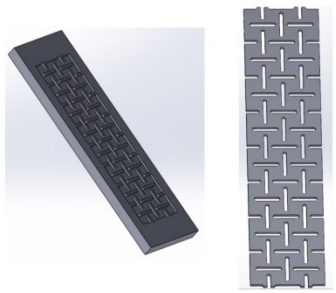

Figure 3: Rotating squares system (SOLIDWORKS)

2.1.3. Wrinkled Structure

The wrinkled structure causes the strain sensor to be highly stretched under mild strain, providing an additional increase in the surface area (length) of the electrodes. Incorporating the wrinkled technique requires only a slight adjustment (Fabrication Process), so it is both time-efficient and cost-efficient. In the unstretched state, the wrinkles appear as tiny, irregular bumps covering the dielectric layer; in the stretched state, each wrinkle gradually smooths out until they are completely unfolded. (Figure 4 and 5)

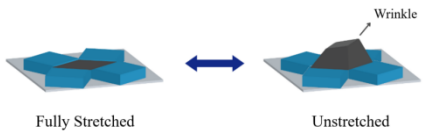

Figure 4: Wrinkle unit

Figure 5: Wrinkled structure

DOI: 10.54254/2753-8818/83/2025.19926

2.2. Material

Silica gel (SiO_2) with a Young's modulus of 750 kPa is used to fabricate the dielectric layer and the ultrathin film. The maximum elongation of inorganic silica gel is 480%, and its operating temperature after curing is -60°C to 250°C.

The electrodes are fabricated from conductive fabric (LessEMF, USA), made of 76% nylon and 24% elastic fiber, with a 99.9% pure silver plating. This medical-grade material can withstand temperatures ranging from 30°C to 90°C.

2.3. Fabrication Process

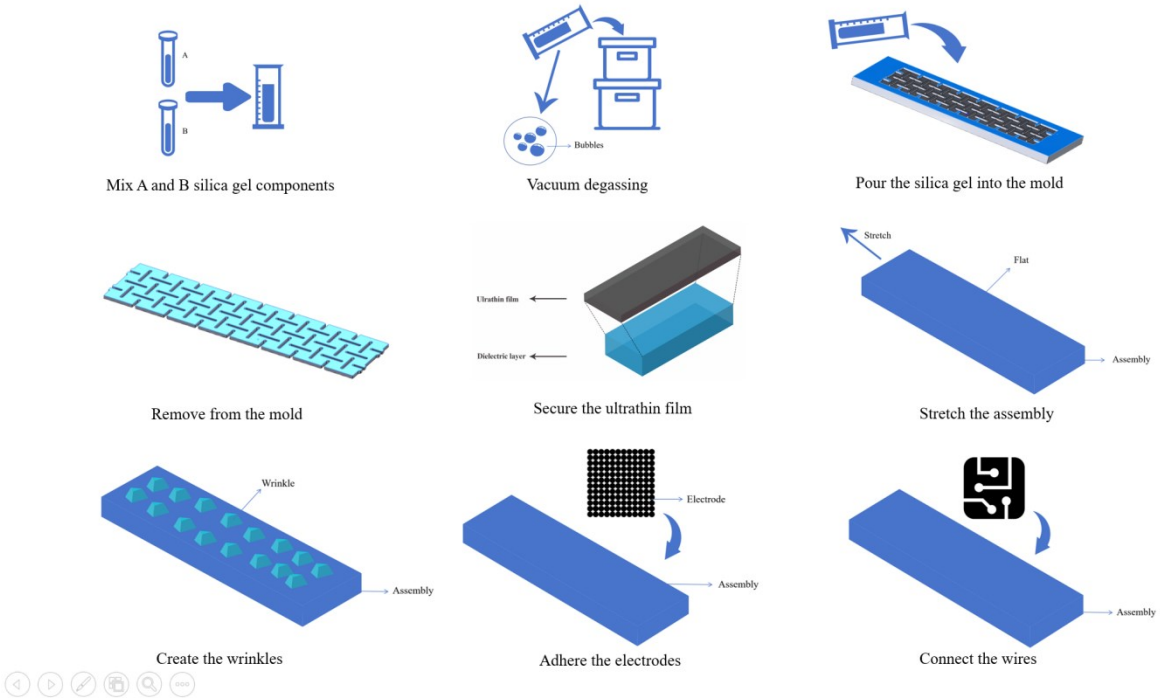

Figure 6: Fabrication process

Figure 6 clearly shows the entire fabrication process. Firstly, the A and B silica gel components are mixed in a 1:1 ratio, and stirred for at least 3 minutes to ensure even mixing. Secondly, the well-mixed materials are placed into a vacuum degassing machine and stirred for ten minutes to eliminate bubbles. Then, the bubble-free mixtures are poured into the molds for the dielectric layer ($80.0\text{mm} * 20.0\text{mm} * 1.0\text{mm}$) and the ultrathin film ($85.0\text{mm} * 20.0\text{mm} * 0.1\text{mm}$), respectively. After allowing the solutions to solidify for 6 hours, the dielectric layer and ultrathin film can be removed from the molds. Subsequently, the four corners of the film are aligned and secured with the four corners of the dielectric layer. Because the film is longer than the dielectric layer, it cannot lie flat against the dielectric layer and instead bulges slightly in the middle. Next, this assembly (including the dielectric layer and film) is stretched by approximately 10% until the film fully attaches to the dielectric layer, and then the film is completely fixed to the dielectric layer. When the stretch is released, the film gradually contracts inward, resulting in the formation of wrinkles. Then, the conductive fabric is adhered to the upper and lower surfaces of the assembly. Finally, the two wires are attached to the upper and lower electrodes, respectively.

DOI: 10.54254/2753-8818/83/2025.19926

3. Model Analysis

3.1. Auxetic Model

Figure 7: Calculation of the Poisson's ratio

The Poisson's ratio of the rotating squares system is expressed as,

$$v_{xy} = (v_{yx})^{-1} = \frac{a^2cos^2(\frac{\theta}{2}) - b^2sin^2(\frac{\theta}{2})}{a^2sin^2(\frac{\theta}{2}) - b^2cos^2(\frac{\theta}{2})} \tag{1}$$

where a represents the sides of the horizontal rectangles, b represents the sides of the vertical rectangles, and θ represents the angle between the rectangles.[17]

When $a = b$ and θ is between 0 and 90 degrees, the equation simplifies to,

$$v_{xy} = \frac{a^2[cos^2(\frac{\theta}{2}) - sin^2(\frac{\theta}{2})]}{a^2[sin^2(\frac{\theta}{2}) - cos^2(\frac{\theta}{2})]} = \frac{cos^2(\frac{\theta}{2}) - sin^2(\frac{\theta}{2})}{sin^2(\frac{\theta}{2}) - cos^2(\frac{\theta}{2})} \tag{2}$$

This can be further simplified to,

$$v_{xy} = \frac{-(sin^2(\frac{\theta}{2}) - cos^2(\frac{\theta}{2}))}{sin^2(\frac{\theta}{2}) - cos^2(\frac{\theta}{2})} = -1 \tag{3}$$

Therefore, the rotating squares system can be theoretically shown to exhibit a huge negative Poisson's ratio -1.

3.2. Capacitive Model

The initial length, width and thickness of the strain sensor is defined as L_0, W_0, d_0. After stretching, these values change to L, W, d. Since the sensor is mainly composed of silica gel, which can be assumed as isotropic incompressible hyperelastic material, its volume and relative permittivity remain constant during stretching.

$$L_0W_0d_0 = LWd \tag{4}$$

Considering the equivalent Poisson's ratio of the entire sensor as v_e, the length of the sensor after stretching is $L_0(1+\varepsilon)$, and the width is $W_0(1 - v_e\varepsilon)d$ (the width will increase since v_e is negative).

$$L_0W_0d_0 = L_0(1+\varepsilon)W_0(1 - v_e\varepsilon)d \tag{5}$$

Rearranging Equation (5), d can be expressed as,

$$d = \frac{d_0}{(1 - v_e\varepsilon)(1+\varepsilon)} \tag{6}$$

DOI: 10.54254/2753-8818/83/2025.19926

The initial capacitance C_0 of the sensor is given as,

$$C_0 = \varepsilon_0 \varepsilon_r \frac{W_0 L_0}{d_0} \tag{7}$$

According to Equation (5) and (6), the capacitance after stretching is,

$$C = \frac{\varepsilon_0 \varepsilon_r W_0 (1-\nu_e \varepsilon) L_0 (1+\varepsilon)}{d} = \frac{\varepsilon_0 \varepsilon_r W_0 (1-\nu_e \varepsilon)^2 L_0 (1+\varepsilon)^2}{d_0} \tag{8}$$

Thus, the theoretical relationship between the capacitance change rate $\frac{\Delta C}{C_0}$ and the strain ε can be obtained.

$$\frac{\Delta C}{C_0} = \frac{C-C_0}{C_0} = (1-\nu_e \varepsilon)^2 (1+\varepsilon)^2 - 1 \tag{9}$$

Expanding Equation (9), we have,

$$\frac{\Delta C}{C_0} = \left(\nu_e^2 - 4\nu_e + 1\right)\varepsilon^2 + \left(2 - 2\nu_e\right)\varepsilon \tag{10}$$

3.3. Joint Model

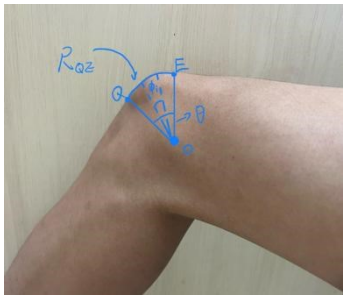

Figure 8: Knee joint

According to the two models mentioned above, a relationship exists between the change in capacitance and the joint bending angle. Taking the knee joint as an example, as illustrated in Figure 8, the left and right endpoints of the knee joint are simplified to points Q and E, respectively. θ represents the bending angle of the knee joint. When θ is equal to 0, the knee is fully extended, and the arc R_{QE} is equal to 0.

To calculate the length of the arc R_{QE}, we can divide it into N segments, each with a constant curvature. Let r_i be the radius of curvature corresponding to any given segment, and φ_i be the central angle corresponding to that segment.

$$R_{QE_i} = r_i \varphi_i \tag{11}$$

During practical testing, the flexible strain sensor is worn on the knee joint. Assuming that bending the knee does not cause any displacement of the sensor, ΔL equals R_{QE}.

$$\Delta L = R_{QE} = \sum_{i=1}^{N} R_{QE} = \frac{1}{\phi} \sum_{i=1}^{N} r_i \varphi_i \cdot \theta \tag{12}$$

Strain ε is defined as,

$$\varepsilon = \frac{\Delta L}{L_0} \tag{13}$$

DOI: 10.54254/2753-8818/83/2025.19926

Therefore, by combining the Equation (12) and (13) with the result (Equation (10)) in capacitive model, we obtain,

$$\frac{\Delta C}{C_0} == \theta^2\left(v_e^2 - 4v_e + 1\right)\left(\frac{\frac{1}{\phi}\sum_{i=1}^{N} r_i\varphi_i}{L_0}\right)^2 + \theta\left(2 - 2V_e\right)\frac{\frac{1}{\phi}\sum_{i=1}^{N} r_i\varphi_i}{L_0} \tag{14}$$

Note that $\frac{1}{\phi}\sum_{i=1}^{N} r_i\varphi_i$ is a constant.

4. Simulation Analysis

4.1. Numerical Analysis

Given that$L_0 = 80.0\,mm, W_0 = 20.0\,mm, d_0 = 1.0\,mm$,the initial capacitance C_0 is approximately 29.70 pF. Since the thicknesses of the upper and lower electrodes and the inorganic silica gel film can be ignored, the Poisson's ratio of the entire sensor can be considered equivalent to the Poisson's ratio of the dielectric layer, which is -1, the theoretical minimum Poisson's ratio. The sensitivity of the sensor is defined as GF (Gauge Factor), which can be expressed as,

$$GF = \frac{\Delta C}{C_0 \varepsilon} \tag{15}$$

Figure 9 shows the GF when $v_e = -1$. Here, we can find that when the strain is 12.50%, the GF value remarkably achieves 4.75. However, simulation testing (FEM Analysis) showed that the Poisson's ratio of the rotating squares system is not exactly equal to -1, but instead ranges from -0.9 to -0.6, depending on the value of ΔL. To obtain more accurate theoretical values, v_e is set to -0.8. The results are shown in Figure 9. It is surprising that the maximum GF value still achieves 4.20 when the Poisson's ratio is -0.8.

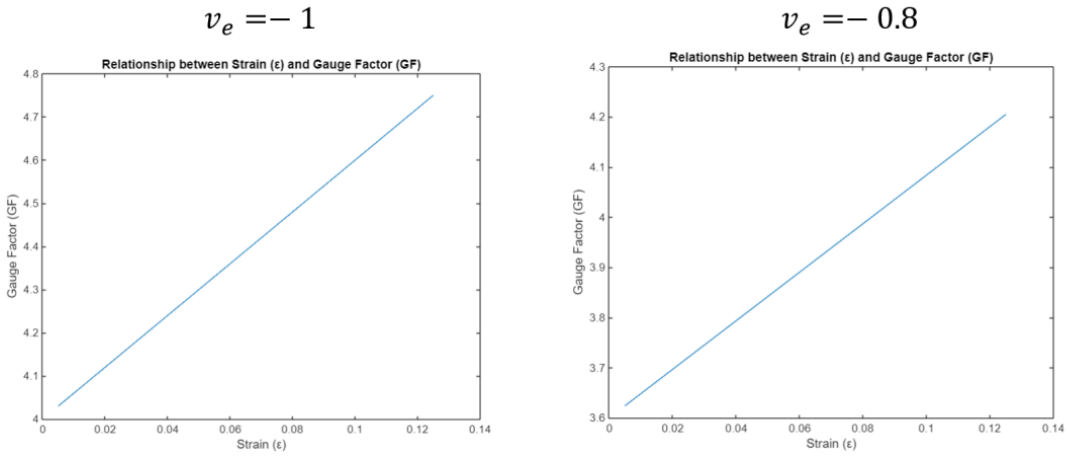

Figure 9: Predicted sensitivity

4.2. FEM Analysis

To test the Poisson's ratio of the rotating squares system during stretching, simulations are conducted using COMSOL. In addition, an anti-tetrachiral structure of the same size is also tested under the same physical conditions for comparison. Figure 10 displays the displacement of the 2D rotating squares system ($80.0mm * 20.0mm$) under different strains, and Figures 11 displays the displacement of the 2D anti-tetrachiral structure ($80.0mm * 20.0mm$) under different strains.

DOI: 10.54254/2753-8818/83/2025.19926

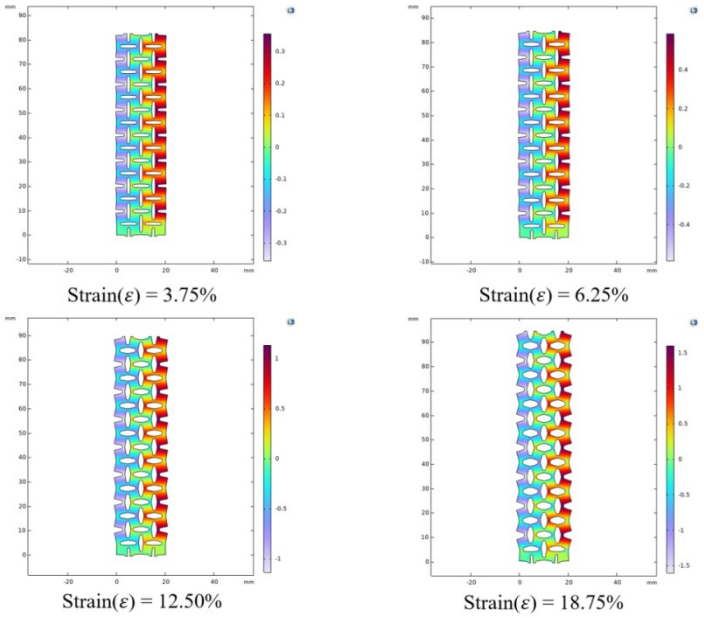

Figure 10: Displacement of the rotating squares system

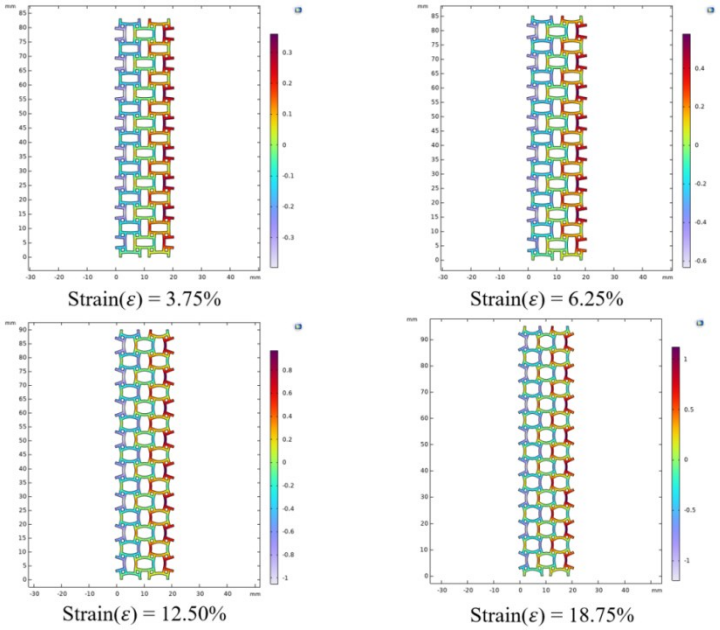

Figure 11: Displacement of the anti-tetrachiral structure

As shown in Tables 1 and 2, although the Poisson's ratio of the rotating squares system does not achieve its theoretical value of -1, it is still significantly better than that of the anti-tetrachiral structure.

Table 1: Calculated Poisson's ratio v_e of the rotating squares system

Case	Strain(ε)	ΔL(mm)	ΔM(mm)	Poisson's ratio(v_e)
Case 1	3.75%	3.00	0.64	-0.85
Case 2	6.25%	5.00	1.05	-0.84
Case 3	12.50%	10.00	2.00	-0.80
Case 4	18.75%	15.00	2.60	-0.69

DOI: 10.54254/2753-8818/83/2025.19926

Table 2: Calculated Poisson's ratio v_e of the anti-tetrachiral structure

Case	**Strain(ε)**	**ΔL(mm)**	**ΔM(mm)**	**Poisson's ratio(v_e)**
Case 1	3.75%	3.00	0.61	-0.81
Case 2	6.25%	5.00	0.94	-0.75
Case 3	12.50%	10.00	1.36	-0.54
Case 4	18.75%	15.00	1.29	-0.34

Note that the Poisson's ratio of the rotating squares system is not stable under different strains, which may result in errors when calculating capacitance.

5. Experiment

5.1. Tensile Test

Table 3 shows the Poisson's ratio of the rotating squares system ($80.0mm * 20.0mm * 1.0mm$) under different strain.

Table 3: Actual Poisson's ratio v_e of the rotating squares system

Case	Strain(ε)	ΔL(mm)	ΔM(mm)	Poisson's ratio(v_e)
Case 1	3.75%	3	1.4	-1.87
Case 2	6.25%	5	1.6	-1.28
Case 3	12.50%	10	2.0	-0.80
Case 4	18.75%	15	3.0	-0.80

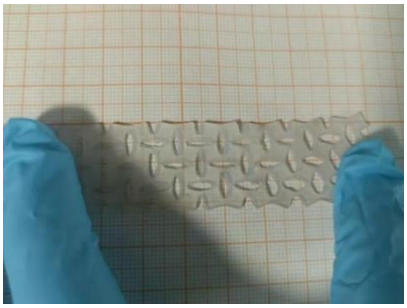

Figure 12: Rotating squares system when stretched

Obviously, The Poisson's ratio increases as the strain increases, eventually stabilizing around -0.8. If the strain exceeds 18.75%, the structure becomes highly susceptible to fracture. This can be attributed to the low thickness of the structure and the fragility of the connections between squares. However, based on the experimental results measuring joint angles (Joint Bending Angles Test), the strain produced by the bending of the knee joint does not exceed 12.50%, together with assistance from the wrinkled structure, so this level of stretchability is completely acceptable.

DOI: 10.54254/2753-8818/83/2025.19926

5.2. Sensitivity Test

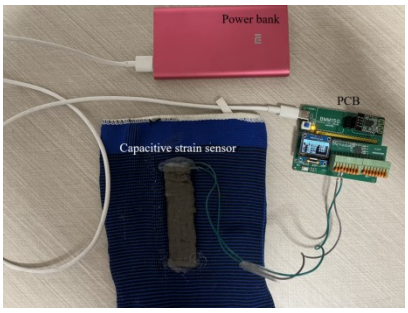

Figure 13: Proposed flexible wearable device

The initial capacitance C_0 is 20.10 pF, which is lower than the theoretical value 29.70 pF. This is because the conductive fabric is difficult to adhere uniformly to wrinkled and auxetic structures. In contrast, electrodes made of other materials, such as liquid metal, are prone to rupture and therefore not suitable for long-term use.

Table 4 shows the change in capacitance ΔC under different strain, and Figure 14 shows the sensitivity (GF) of the sensor.

Table 4: Relationship between the strain and change in capacitance

Case	Strain(ε)	ΔL(mm)	C(pF)	Δ(pF)
Case 1	1.25%	1.00	22.82	2.72
Case 2	2.50%	2.00	24.03	3.93
Case 3	5.00%	4.00	26.08	5.98
Case 4	7.50%	6.00	27.44	7.34
Case 5	10.00%	8.00	28.45	8.35
Case 6	12.50%	10.00	30.32	10.22

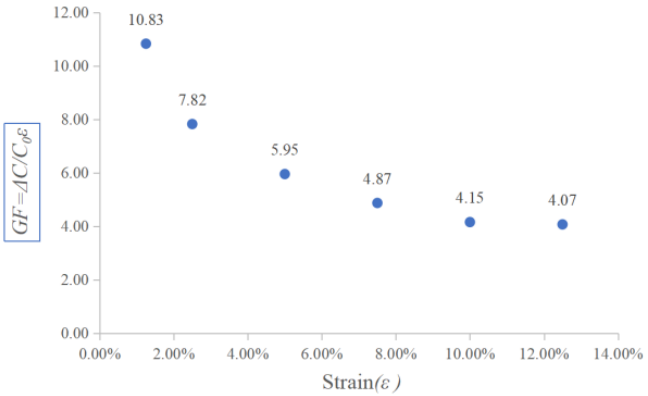

Figure 14: Relationship between the strain and GF

At best, the strain sensor achieves a maximum gauge factor of 10.83 at 1.25% strain and a minimum gauge factor of 4.07 at 12.50% strain, significantly higher than the theoretical maximum gauge factor of 1. Compared to the result in Numerical Analysis, the GF decreases as the strain increases because the Poisson's ratio decreases instead of remaining the same.

Based on the results of Tensile Test, it can be observed that if the strain ($\varepsilon > 12.5\%$) is further increased, the gauge factor (GF) will remain stable around 4 due to the Poisson's ratio stabilizing around -0.8. However, once the strain exceeds 18.75%, the dielectric layer will likely to rupture,

DOI: 10.54254/2753-8818/83/2025.19926

causing a rapid decrease in GF. Therefore, when using this type of capacitive sensor for joint measurements in practical applications, it is crucial to exercise caution and avoid imposing excessive strain.

5.3. Joint Bending Angles Test

5.3.1. Static Test

As seen in Figure 15, the capacitive strain sensor is attached to a knee brace, with the PCB secured to the thigh using a rubber band, and the power bank is placed in a pocket. This method of wearing is quite convenient; however, the knee brace tends to shift easily during testing, which requires frequent adjustments during testing.

Figure 15: Wearing the flexible device

When the knee is fully extended ($\Delta\theta = 0^{\circ}$), the measured capacitance is 20.47 pF, which is approximately equal to the initial capacitance C_0 (20.1 pF). Table 5 shows the relationship between the change in capacitance (ΔC) and the knee's bending angle ($\Delta\theta$).

Table 5: Relationship between the change in capacitance and knee's bending angle

ΔC(pF)	**Δθ**
1.60	10°
4.20	30°
6.00	45°
7.10	60°
9.10	90°

Note that when the knee is bent at a 90-degree angle, the change in capacitance reaches 9.10 pF, which is less than the 10.22 pF achieved at a 12.5% strain (Sensitivity Test).

5.3.2. Dynamic Test

Figure 17 shows the angles of the knee joint during walking (**Figure 16**), ranging from 19° to 62°. When $\Delta\theta$ is greater than 50°, the tested leg is about to step forward but has not yet completely left the ground. When $\Delta\theta$ is less than 25°, the tested leg is acting as the supporting leg and is mostly straight.

Figure 16: Walking with the proposed device

DOI: 10.54254/2753-8818/83/2025.19926

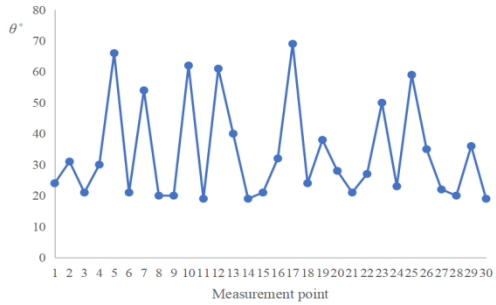

Figure 17: Angles of the knee joint (walking)

Figure 18: Jumping with the proposed device

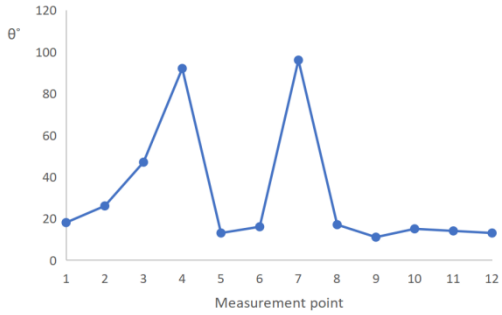

Figure 19: Angles of the knee joint (jumping with both feet)

Figure 19 shows the angles of the knee joint (left knee) during a jump with both feet (Figure 18), ranging from 17° to 96°. When the experimenter begins to squat, $\Delta\theta$ increases rapidly. As he pushes off to jump up, $\Delta\theta$ quickly decreases. During the airborne phase, the knee is almost fully extended, causing $\Delta\theta$ to remain at a very low value. When landing, the experimenter bends his knees to absorb the impact, causing $\Delta\theta$ to rise again rapidly. When the experimenter stands back up, $\Delta\theta$ returns to its initial value.

Figure 20: Jump shot with the proposed device

DOI: 10.54254/2753-8818/83/2025.19926

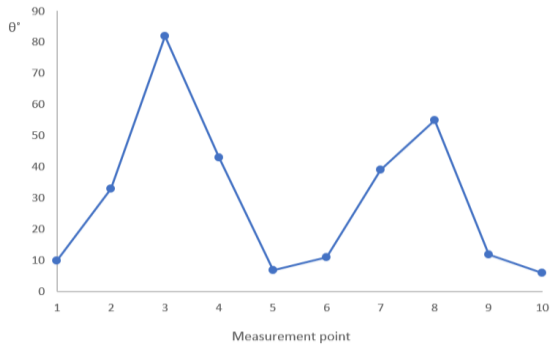

Figure 21: Angles of the knee joint (jump shot)

Figure 21 shows the angles of the knee joint during a jump shot (Figure 20), ranging from 6° to 82°. When the experimenter squats down, $\Delta\theta$ increases until the experimenter prepares to jump. As the experimenter jumps up, $\Delta\theta$ rapidly decreases until he lands and starts bending his knees again. At this moment, $\Delta\theta$ rises once more. Finally, when the experimenter extends his knees, $\Delta\theta$ gradually decreases back to zero.

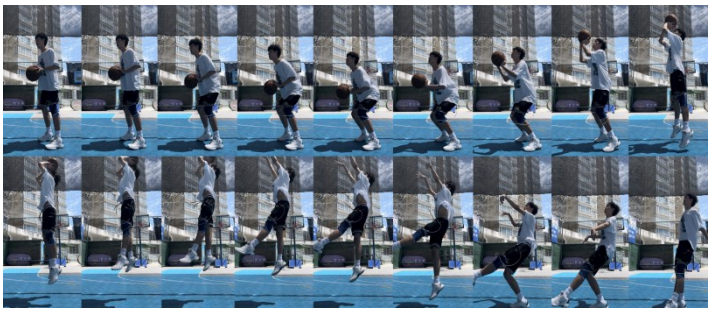

Figure 22: Fadeaway with the proposed device

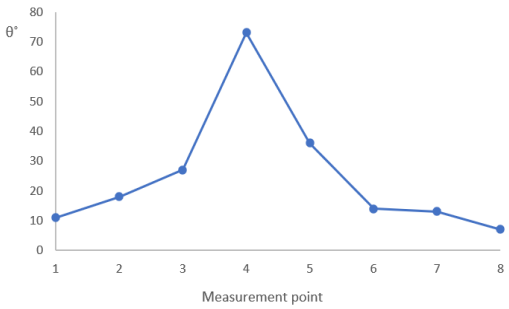

Figure 23: Angles of the knee joint (fadeaway)

Figure 23 shows the angles of the knee joint during a fadeaway (Figure 22), ranging from 7° to 73°. The trend of $\Delta\theta$during squatting and jumping is generally consistent with $\Delta\theta$ observed in a jump shot. However, during a fadeaway, the tested leg (left leg) extends forward to maintain balance, causing the right leg to land first and bend. As a result, the left leg tends to keep straight, and $\Delta\theta$ does not increase again.

6. Conclusion

This study presents a novel configuration for capacitive strain sensors that are used for tracking joint bending angles at low-strain levels, which achieves a maximum gauge factor of 10.83 at 1.25% strain

DOI: 10.54254/2753-8818/83/2025.19926

and a minimum gauge factor of 4.07 at 12.50% strain, considerably higher than the theoretical value 1. Compared to the approach proposed by Jun Shintake et al. (2019), which integrates the auxetic structure into the upper and lower surfaces of the electrodes, directly replacing the traditional dielectric layer with the auxetic and wrinkled structure proves to be more effective in enhancing sensitivity.[18]

Due to its higher sensitivity under low strain, this configuration is more optimal for measuring joint angles in areas other than the knee, such as the cervical spine, ankle, elbow, wrist, and fingers. Its gauge factor, which remains above 4, offers significant advantages in applications like sports training, injury prevention and sports rehabilitation. For example, this strain sensor could be used to track the angles of the elbow, wrist, and fingers simultaneously with exceptional accuracy when a basketball player is performing a shooting motion.

References

[1] *Du, Qianchao. (2024). Dynamic Monitoring System for Wearable Devices in Human Motion Based on Augmented Reality. Automation and Instrumentation, (02), 140-144. doi:10.14016/j.cnki.1001-9227.2024.02.140.*

[2] *Lee, H. J., Lee, S., Chang, W. H., Seo, K., Shim, Y., Choi, B. O., ... & Kim, Y. H. (2017). A wearable hip assist robot can improve gait function and cardiopulmonary metabolic efficiency in elderly adults. IEEE transactions on neural systems and rehabilitation engineering, 25(9), 1549-1557.*

[3] *Bolam, S. M., Batinica, B., Yeung, T. C., Weaver, S., Cantamessa, A., Vanderboor, T. C., ... & Monk, A. P. (2021). Remote patient monitoring with wearable sensors following knee arthroplasty. Sensors, 21(15), 5143.*

[4] *Kuptniratsaikul, V., Kovindha, A., Suethanapornkul, S., Massakulpan, P., Permsirivanich, W., & Kuptniratsaikul, P. S. A. (2017). Motor recovery of stroke patients after rehabilitation: one-year follow-up study. International Journal of Neuroscience, 127(1), 37-43.*

[5] *Ramkumar, P. N., Haeberle, H. S., Ramanathan, D., Cantrell, W. A., Navarro, S. M., Mont, M. A., ... & Patterson, B. M. (2019). Remote patient monitoring using mobile health for total knee arthroplasty: validation of a wearable and machine learning–based surveillance platform. The Journal of arthroplasty, 34(10), 2253-2259.*

[6] *Amjadi, M., Kyung, K. U., Park, I., & Sitti, M. (2016). Stretchable, skin‐mountable, and wearable strain sensors and their potential applications: a review. Advanced Functional Materials, 26(11), 1678-1698.*

[7] *Dong, T., Gu, Y., Liu, T., & Pecht, M. (2021). Resistive and capacitive strain sensors based on customized compliant electrode: Comparison and their wearable applications. Sensors and Actuators A: Physical, 326, 112720.*

[8] *Shintake, J., Piskarev, Y., Jeong, S. H., & Floreano, D. (2018). Ultrastretchable strain sensors using carbon black‐filled elastomer composites and comparison of capacitive versus resistive sensors. Advanced Materials Technologies, 3(3), 1700284.*

[9] *Kim, S. R., Kim, J. H., & Park, J. W. (2017). Wearable and transparent capacitive strain sensor with high sensitivity based on patterned Ag nanowire networks. ACS applied materials & interfaces, 9(31), 26407-26416.*

[10] *Nur, R., Matsuhisa, N., Jiang, Z., Nayeem, M. O. G., Yokota, T., & Someya, T. (2018). A highly sensitive capacitive-type strain sensor using wrinkled ultrathin gold films. Nano letters, 18(9), 5610-5617.*

[11] *Hu, X., Yang, F., Wu, M., Sui, Y., Guo, D., Li, M., ... & Liu, J. (2022). A super‐stretchable and highly sensitive carbon nanotube capacitive strain sensor for wearable applications and soft robotics. Advanced Materials Technologies, 7(3), 2100769.*

[12] *Ren, X., Das, R., Tran, P., Ngo, T. D., & Xie, Y. M. (2018). Auxetic metamaterials and structures: a review. Smart materials and structures, 27(2), 023001.*

[13] *Li, Y., Luo, S., Yang, M. C., Liang, R., & Zeng, C. (2016). Poisson ratio and piezoresistive sensing: a new route to high‐performance 3D flexible and stretchable sensors of multimodal sensing capability. Advanced Functional Materials, 26(17), 2900-2908.*

[14] *Taherkhani, B., Azizkhani, M. B., Kadkhodapour, J., Anaraki, A. P., & Rastgordani, S. (2020). Highly sensitive, piezoresistive, silicone/carbon fiber-based auxetic sensor for low strain values. Sensors and Actuators A: Physical, 305, 111939. Jun Shintake, et al., (2019), Sensitivity Improvement of Highly Stretchable Capacitive Strain Sensors by Hierarchical Auxetic Structures*

[15] *Wang, Z., Luan, C., Liao, G., Liu, J., Yao, X., & Fu, J. (2021). High-performance auxetic bilayer conductive mesh-based multi-material integrated stretchable strain sensors. ACS Applied Materials & Interfaces, 13(19), 23038-23048.*

[16] *Mizzi, L., Azzopardi, K. M., Attard, D., Grima, J. N., & Gatt, R. (2015). Auxetic metamaterials exhibiting giant negative Poisson's ratios. physica status solidi (RRL)–Rapid Research Letters, 9(7), 425-430.*

DOI: 10.54254/2753-8818/83/2025.19926

[17] *Grima, J. N., & Gatt, R. (2010). Perforated sheets exhibiting negative Poisson's ratios. Advanced engineering materials, 12(6), 460-464.*

[18] *Shintake, J., Nagai, T., & Ogishima, K. (2019). Sensitivity improvement of highly stretchable capacitive strain sensors by hierarchical auxetic structures. Frontiers in Robotics and AI, 6, 127.*